IL NUOVO CIMENTO Vol. 36 C, N. 5 Settembre-Ottobre 2013
DOI 10.1393/ncc/i2013-11560-0

Colloquia: QCDN12

Nucleon structure using lattice QCD

C. Alexandrou(1)(2), M. Constantinou(1), V. Drach(3), K. Hadjiyiannakou(1), K. Jansen(3)(1), C. Kallidonis(1)(2), G. Koutsou(2), T. Leontiou(4) and A. Vaquero(2)

(1) *Department of Physics, University of Cyprus - PO Box 20537, 1678 Nicosia, Cyprus*
(2) *Computational-based Science and Technology Research Center, The Cyprus Institute P.O. Box 27456, CY-1645 Nicosia, Cyprus*
(3) *NIC, DESY - Platanenallee 6, D-15738 Zeuthen, Germany*
(4) *General Department, Frederick University - 1036 Nicosia, Cyprus*

ricevuto il 18 Aprile 2013

Summary. — A review of recent nucleon structure calculations within lattice QCD is presented. The nucleon excited states, the axial charge, the isovector momentum fraction and helicity distribution are discussed, assessing the methods applied for their study, including approaches to evaluate the disconnected contributions. Results on the spin carried by the quarks in the nucleon are also presented.

PACS 11.15.Ha – Lattice gauge theory.
PACS 12.38.Gc – Lattice QCD calculations.
PACS 13.40.Gp – Electromagnetic form factors.

1. – Introduction

During the last decade, results from simulations of QCD have emerged that already provide essential input for a wide range of strong interaction phenomena as, for example, the QCD phase diagram, the structure of hadrons, nuclear forces and weak decays. In this presentation, we focus on hadron structure calculations using state-of-the art lattice QCD simulations [1-3].

Understanding nucleon structure from first principles is considered a milestone of hadronic physics. A rich experimental program has been devoted to its study, starting with the measurements of the electromagnetic nucleon form factors initiated more than 50 years ago. Reproducing these key observables within the lattice QCD formulation is a prerequisite for obtaining reliable predictions on observables that explore physics beyond the standard model. In particular we discuss three fundamental quantities, which can be easily extracted from nucleon matrix element calculations on the lattice, namely the nucleon axial charge, the isovector momentum fraction and the helicity moment. The reason for this choice is that they are known experimentally and they all can be directly determined at momentum transfer squared $q^2 = 0$. Thus there is no ambiguity associated

with having to fit the q^2-dependence of the form factor (FF), as for example, in the case of the anomalous magnetic moment where one needs to fit the small q^2-dependence of the magnetic FF. In addition, only the connected diagram, for which established lattice methods exist for its calculation, contributes.

For the discussion of the spin content of the nucleon however, one needs to calculate the contributions carried by the u- and d-quarks. Contributions from fermion loops need to be taken into account in this case. There are on-going efforts to compute these so called disconnected contributions, which will be briefly discussed here. However, in the final results shown in this work for the quark spin these contributions will be neglected.

2. – Methodology

It is convenient to decompose the nucleon matrix elements, $\langle N(p',s')|\mathcal{O}_\Gamma^{\mu\mu_1\cdots\mu_n}|N(p,s)\rangle$, into generalized form factors (GFFs) as follows:

$$(1)\quad u_N(p',s')\Bigg[\sum_{i=0,2,\ldots}^{n}\left(A_{n+1,i}(q^2)\gamma^{\{\mu}+B_{n+1,i}(q^2)\frac{i\sigma^{\{\mu\alpha}q_\alpha}{2m}\right)q^{\mu_1}\ldots q^{\mu_i}\overline{P}^{\mu_{i+1}}\ldots\overline{P}^{\mu_n\}} +\mathrm{mod}(n,2)C_{n+1,0}(q^2)\frac{1}{m}q^{\{\mu}q^{\mu_1}\ldots q^{\mu_n\}}\Bigg]u_N(p,s).$$

For $p'=p$ one has the n^{th} moment of the unpolarized parton distribution, $\langle x^n\rangle_q$. A similar expression can be written for $\mathcal{O}_{\Delta q}^{\mu\mu_1\cdots\mu_n}$ in terms of $\tilde{A}_{ni}(q^2)$ and $\tilde{B}_{ni}(q^2)$. The ordinary nucleon form factors are then special cases of GFFs given by

$$(2)\quad A_{10}(q^2)=F_1(q^2)=\int_{-1}^{1}\mathrm{d}xH(x,\xi,q^2),\qquad B_{10}(q^2)=F_2(q^2)=\int_{-1}^{1}\mathrm{d}xE(x,\xi,q^2),$$
$$\tilde{A}_{10}(q^2)=G_A(q^2)=\int_{-1}^{1}\mathrm{d}x\tilde{H}(x,\xi,q^2),\qquad \tilde{B}_{10}(q^2)=G_p(q^2)=\int_{-1}^{1}\mathrm{d}x\tilde{E}(x,\xi,q^2),$$

while $A_{n0}(0)$, $\tilde{A}_{n0}(0)$, $A_{n0}^T(0)$ are moments of parton distributions, *e.g.* $\langle x\rangle_q=A_{20}(0)$ and $\langle x\rangle_{\Delta q}=\tilde{A}_{20}(0)$ are the first moments of the spin independent and helicity distributions. With knowledge of these moments, one can evaluate the quark contributions to the nucleon spin using the decomposition $J_q=\frac{1}{2}[A_{20}(0)+B_{20}(0)]=\frac{1}{2}\Delta\Sigma+L_q$ and $\Delta\Sigma=\tilde{A}_{10}$. The nucleon spin sum rule $\frac{1}{2}=\frac{1}{2}\Delta\Sigma+L_q+J_g$ allows the determination of the gluon contribution J_g.

In lattice QCD, one proceeds with the calculation of nucleon matrix elements, by creating a state with the quantum numbers of the nucleon J_N^α at an initial time, $t_i=0$ (source), inserting a current at some intermediate time, t, and subsequently annihilating the nucleon at the final time, t_f, (sink). Such a three-point function is shown in figs. 1 and 2, where the lines represent fully dressed quark propagators. For a general operator $\mathcal{O}_\Gamma$, one is interested in the momentum-dependent matrix element:

$$(3)\quad G^{\mu\mu_1\cdots\mu_n}(\Gamma^\nu;t_f;t;\vec{q})=\sum_{\vec{x}_f,\vec{x}_i}\Gamma^\nu_{\beta\alpha}\langle J_N^\alpha(\vec{x}_f,t_f)\mathcal{O}^{\mu\mu_1\cdots\mu_n}(\vec{x},t)\bar{J}_N^\beta(\vec{0},0)\rangle e^{-i\vec{q}\cdot\vec{x}},$$

where the projection matrices Γ^ν are $\Gamma_0=\frac{1}{4}(1+\gamma_0)$, $\Gamma_k=i\Gamma_0\gamma_5\gamma_k$, $k=1,2,3$. Depending on the quark structure of the operator $\mathcal{O}_\Gamma$, such a matrix element is a combination of connected and disconnected contributions, as shown in figs. 1 and 2, respectively.

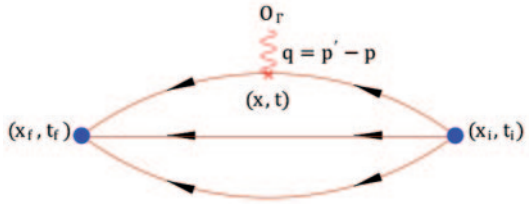

Fig. 1. – Connected contribution to a baryon 3-point function.

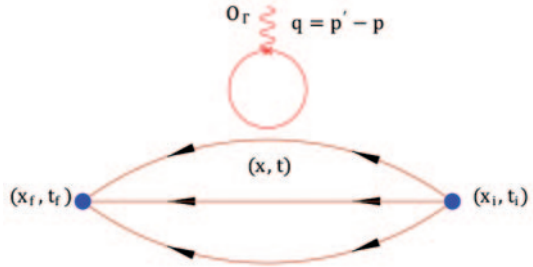

Fig. 2. – Disconnected contribution to a baryon 3-point function.

The nucleon matrix element is obtained in the limit where the time separation between the current insertion and the source and the sink are large enough such that only the ground state matrix element dominates. An appropriately defined ratio

$$(4)\quad R^{\mu}(\Gamma^{\nu};t_f;t;\vec{q}) = \frac{G^{\mu}(\Gamma^{\nu};t_f;t;\vec{q})}{G(\vec{0},t_f)}\sqrt{\frac{G(\vec{q},t_f-t)G(\vec{0},t)G(\vec{0},t_f)}{G(\vec{0},t_f-t)G(\vec{q},t)G(\vec{q},t_f)}} \xrightarrow[t_f-t\gg 1]{t\gg 1} \Pi^{\mu}(\Gamma^{\nu};\vec{q})$$

thus becomes time independent ("plateau region") and unknown overlaps of the nucleon state with the trial states are canceled. In eq. (4) we have taken the final momentum

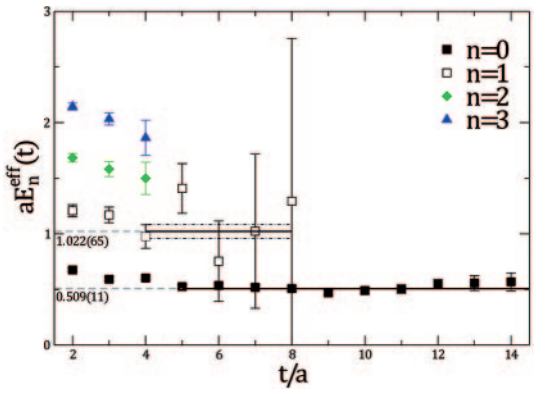

Fig. 3. – The four lowest states of the nucleon in the positive parity channel extracted using $N_f = 2$ twisted mass fermions (TMF) with pion mass 308 MeV. The solid lines and bands show the value and error extracted from a fit in the plateau region.

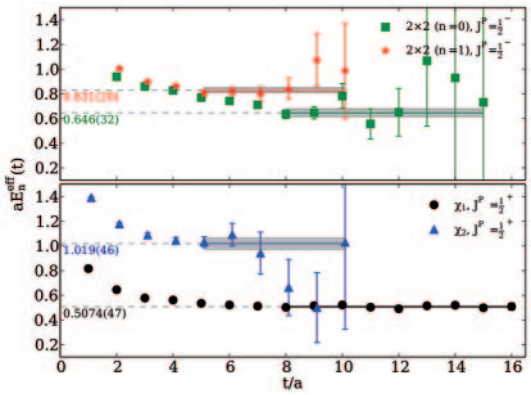

Fig. 4. – The two lowest states of the nucleon in the positive (lower) and negative (upper) parity channels using two dynamical flavors ($N_f = 2$) of TMF gauge ensembles with pion mass 308 MeV.

$\vec{p}\,' = 0$. The two-point function appearing in eq. (4) is given by

$$G(\vec{q}, t_f) = \sum_{\vec{x}_f} \Gamma_0^{\beta\alpha} \langle J_N^{\alpha}(\vec{x}_f, t) \bar{J}_N^{\beta}(\vec{0}, 0) \rangle e^{-i\vec{q}\cdot\vec{x}_f}. \tag{5}$$

Energies of hadronic states are extracted from two-point functions by taking the ratio $E_{\text{eff}}(t) = \log[G(\vec{0}, t)/G(\vec{0}, t+1)] \to E_0$. Utilizing a basis of interpolating fields $J_N(x)$ one can extract both the ground state and excited states. In fig. 3 we show an example of utilizing a five-dimensional basis of interpolators to extract the excited states of the nucleon in the positive parity channel. As can be seen, identifying a plateau region is crucial to reliably extract the energy of excited states. Using more suitable interpolating fields can improve the plateaus as shown in fig. 4 for both the positive and negative parity channels.

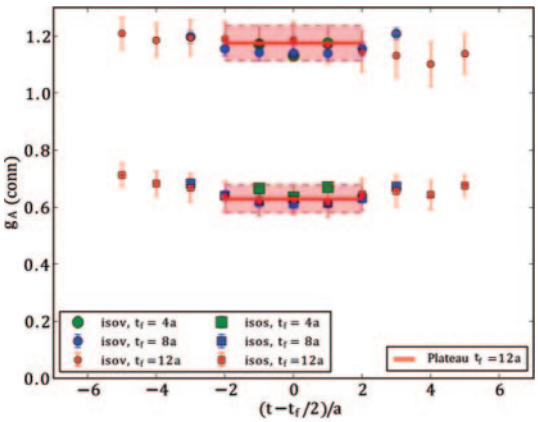

Fig. 5. – The nucleon matrix element of the isovector (isov) and the connected contribution to the isoscalar (isos) axial-vector operator. The solid line shows the fit to a constant.

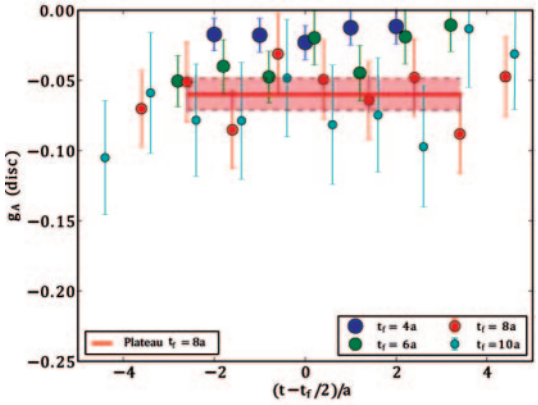

Fig. 6. – The disconnected contribution to the nucleon matrix element of the isoscalar axial operator as a function of the insertion time-slice. The solid line shows the fit to a constant.

Unlike the case of the isovector nucleon matrix elements, where quark disconnected contributions cancel, for the isoscalar case, both connected and disconnected quark diagrams contribute. These contributions are shown in fig. 5, for the case of the isoscalar nucleon matrix element of the axial-vector current at $q^2 = 0$. Results for the ratio of eq. (4) are shown for various source-sink time separations. When the ground state dominates there is convergence of the results obtained for various source-sink time separations.

The disconnected diagrams are notoriously difficult to compute because they exhibit large statistical errors and require knowledge of all elements of the quark propagator. The so-called all-to-all propagator is impractical to compute and store explicitly. Stochastic techniques are typically employed to obtain estimates of the all-to-all propagator combined with techniques to efficiently multiply the number of measurements to suppress the statistical uncertainty. Such calculations have been shown to be especially suited for GPUs [4, 5]. In fig. 6 we show the disconnected contribution to the isoscalar nucleon matrix element of the axial-vector current for various source-sink separations. Note the much larger errors as compared to those obtained from the connected part.

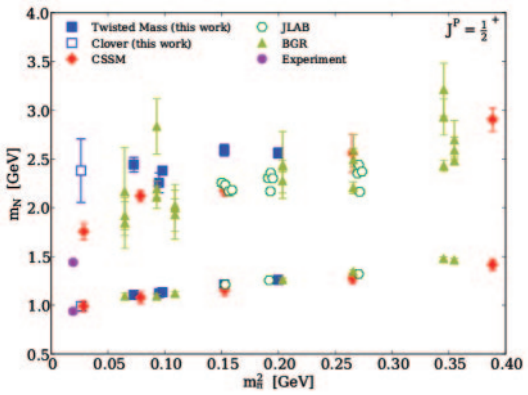

Fig. 7. – The positive parity states of the nucleon using twisted mass and clover fermions from various groups. The magenta filled circles show the experimental values of the nucleon mass and the Roper.

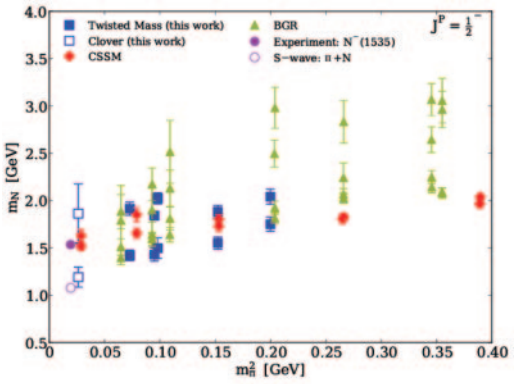

Fig. 8. – The negative parity states of the nucleon using twisted mass and clover fermions from various groups. The filled magenta circle shows the $S_{11}(1535)$, whereas the open magenta circle the πN mass.

3. – Results

The spectrum of the nucleon is explored by several groups. In figs. 7 and 8 we show recent results on the first excited states of the nucleon [6]. All lattice results are in nice agreement for the ground state. Results for the first excited state show larger statistical errors and deviations. Most lattice data are higher than the mass of the Roper, even when pion masses at almost the physical value are used. This is currently under investigation. In the negative parity channel, lattice results give the experimental value of the $S_{11}(1535)$.

Reproducing the nucleon axial charge is important for benchmarking our lattice QCD formulation beyond reproducing masses of low-lying hadrons. We show in fig. 9, the axial charge of the nucleon g_A, extracted from fitting to the plateau region of the ratio of eq. (4) and which uses the isovector current for which disconnected contributions cancel. The first observation is the consistency between different lattice formulations. This consistency is non-trivial, since the results shown are at different, non-zero lattice spacings, and in general these different formulations have different finite-spacing correction terms. Furthermore, all results underestimate the experimental value as the pion mass

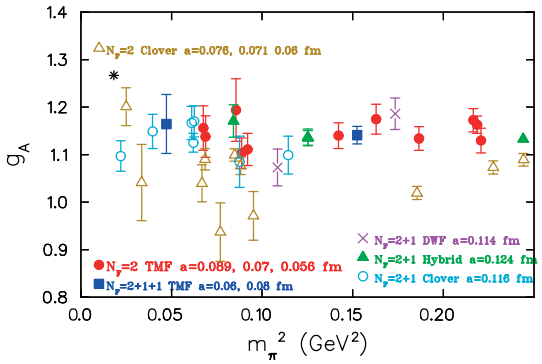

Fig. 9. – Lattice results on the axial charge of the nucleon for: $N_f = 2$ and $N_f = 2 + 1 + 1$ TMF [7]; $N_f = 2 + 1$ DWF [8]; hybrid [9]; $N_f = 2$ clover [10]; $N_f = 2 + 1$ clover [11]. The physical point is shown by the asterisk.

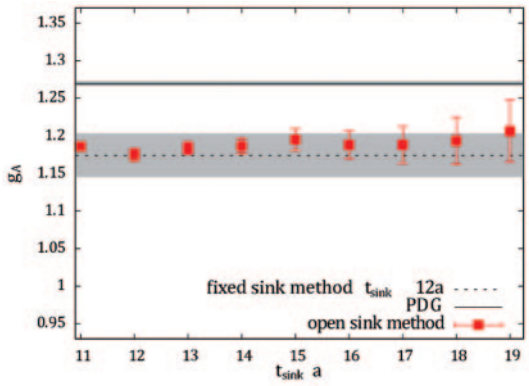

Fig. 10. – The value of g_A versus the sink-source time separation ($N_f = 2 + 1+$ TMF at ~ 350 MeV.

approaches its physical value. Candidates for this discrepancy are currently thought to be systematic effects in lattice calculations, such as artifacts caused by the finite volume or contamination of the matrix element by excited states. The latter has been investigated thoroughly in a high statistics calculation [12]. As can be seen in fig. 10, g_A does not suffer from excited state contamination since the plateau value remains consistent for a large range of source-sink separations. This conclusion is consistent with fig. 5. An alternative to fitting the plateau of eq. (4) is the summation method that modifies the excited state contributions [13, 14]. Further sources of systematic uncertainties are currently under investigation by various lattice QCD Collaborations.

In fig. 11 we show the isovector combination for the momentum fraction $A_{20}(0) = \langle x \rangle_{u-d}$ for various fermion discretization schemes. The general conclusion is again that lattice results are in agreement among themselves, a strong indication that finite lattice spacing corrections are smaller than the statistical errors. Results at almost physical pion mass in this case appear to be converging to the physical point. Confirmation of this trend is on-going with computations being performed at near physical pion mass and large volumes. In fig. 12 we show results for the helicity $\tilde{A}_{20}(0) = \langle x \rangle_{\Delta u - \Delta d}$. The situation is very similar to the momentum fraction.

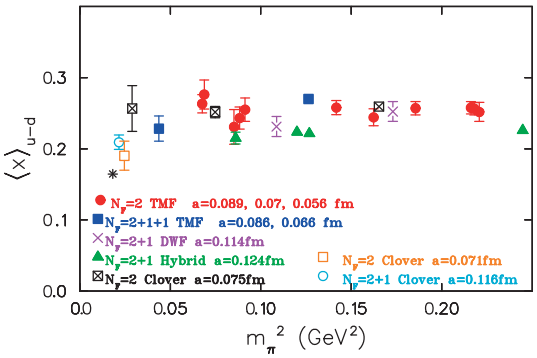

Fig. 11. – Lattice results on the isovector momentum fraction $\langle x \rangle_{u-d}$ of the nucleon. The crosses, crossed and open squares are from refs. [15-17], respectively. The rest of the notation is the same as that in fig. 9.

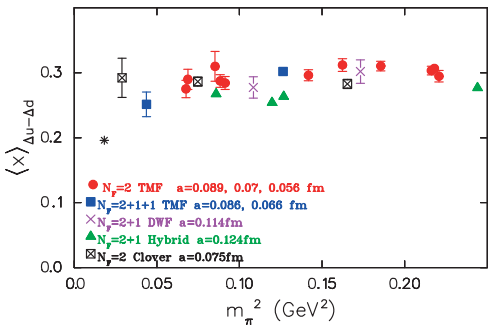

Fig. 12. – Lattice results on the isovector polarized moment $\langle x \rangle_{\Delta u - \Delta d}$ of the nucleon. The notation is the same as that in fig. 11.

The matrix elements presented so far are directly related to the contribution of the nucleon constituent quarks to its spin, as explained in the introduction. Knowledge of both isovector and isoscalar combinations are required in order to obtain the individual quark contributions. From here on, we ignore disconnected contributions to the isoscalar matrix elements. There are indications that their contributions are small, *e.g.* for the case of $g_A = \tilde{A}_{10}(0)$ these are expected to be of the order of 10%, as can be seen from fig. 6. Calculations are underway for their precise determination. The total angular momentum carried by quarks requires knowledge of $B_{20}(0)$, which on the lattice cannot be obtained at zero momentum transfer. $B_{20}(0)$ is therefore calculated by fitting the momentum dependence, for which we assume a linear form.

We show in fig. 13 the quark contributions to the proton spin. We compare results obtained using $N_f = 2$ and $N_f = 2+1+1$ TMF with those using a hybrid action of $N_f = 2+1$ staggered sea and domain wall valence quarks [9]. As can be seen, the total spin carried by the u- and d-quarks $J^{u+d} \sim J^u$ since $J^d \sim 0$. This can be traced to the intrinsic spin $\frac{1}{2}\Delta\Sigma^d$ and angular momentum L^d of the d-quarks canceling.

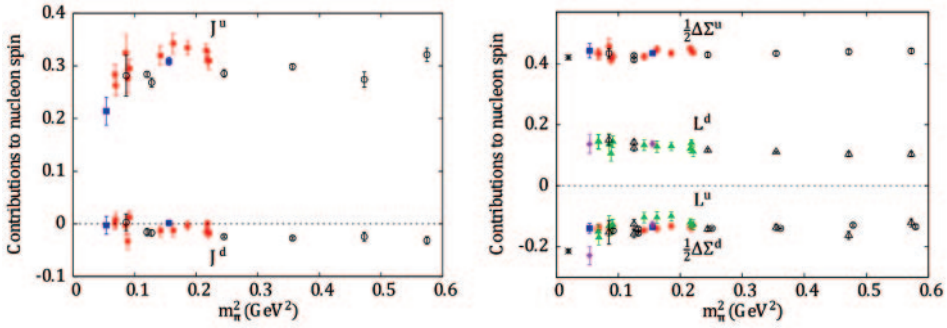

Fig. 13. – Quark contributions to the proton spin as a function of the pion mass. Left: the total contributions of the up- and down-quarks (J^u and J^d respectively). Filled squares are obtained using $N_f = 2+1+1$ TMF, filled circles using $N_f = 2$ TMF, compared to results obtained using a hybrid action [9] (open symbols). Right: The quark spin and quark orbital angular momentum contribution to the nucleon spin obtained using $N_f = 2+1+1$ twisted mass fermions (filled squares and diamonds respectively), using $N_f = 2$ twisted mass fermions (filled circles and triangles respectively) and using a hybrid action (open circles and open triangles respectively). Asterisks denote the experimental results.

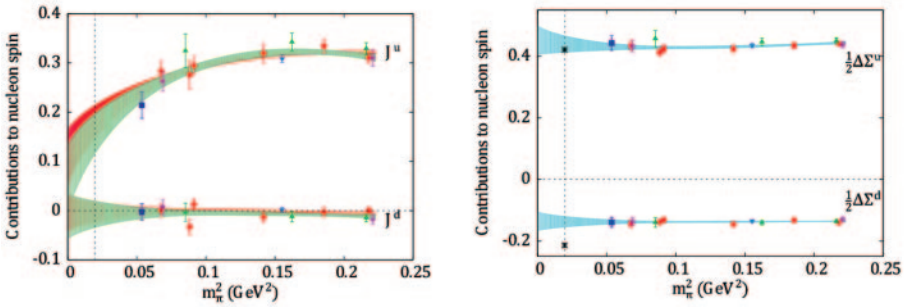

Fig. 14. – Chiral extrapolation of the quark contributions to the proton spin. The vertical line denotes the physical point. The data are obtained using $N_f = 2$ twisted mass with $a = 0.089$, 0.07 and 0.056 fm (red circles, green triangles and magenta diamonds), and $N_f = 2 + 1 + 1$ twisted mass with $a = 0.086$ and 0.066 fm (blue inverted triangles and blue squares).

To obtain some insight on the spin carried by the quarks at the physical point we use Heavy Baryon Chiral Perturbation Theory (HBχPT) to extrapolate the lattice data. The expressions for these fits are given in ref. [7], where also covariant χPT was used giving qualitatively similar results. A source of systematic error may came from the fact that $B_{20}(0)$ is obtained via a fit. This is done by extrapolating the data obtained by using two fit ranges in the fit to $B_{20}(Q^2)$, shown by the red and green bands in fig. 14. As can be seen both fit ranges yield consistent results. For the case of the intrinsic spin where experimental data are available, a comparison shows that the down-quark contribution is under estimated, while for the u-quark there is agreement. However, this disagreement is too small to account for the missing 50% of the spin of the nucleon. Disconnected contributions to the quark spins are also expected to be small and therefore a large fraction of the proton spin is not carried by the quarks.

4. – Conclusions

A review of recent lattice QCD nucleon structure calculations is presented, comparing the results obtained by different groups. The nucleon first excited states are presented with good agreement with experiment in the negative parity channel but still not being conclusive in the case of the Roper. Lattice QCD data on the nucleon axial charge are in agreement among themselves but, however, underestimate the experimental value for g_A believed to be due to systematic effects appearing in lattice computations. This calls for an in depth study to identify possible sources of this discrepancy, something which is being investigated currently by several lattice groups. Lattice data for the momentum fraction and helicity on the other hand are seen to converge towards the experimental value as the pion mass decreases below 250 MeV although still remain higher. Recent results near the physical point have suggested excited states [14] to be the source for the remaining discrepancy. This is being investigated.

The axial charge, combined with the momentum fraction, give insight on the fraction of the nucleon spin carried by quarks. Using both isovector and isoscalar combinations of these quantities, with a cautionary remark on the omission of disconnected diagrams that contribute to the latter, we extract the individual up- and down-quark contributions to the proton spin. Qualitatively, we find agreement with what is observed experimentally for the quark intrinsic spin fractions. Recent lattice calculations also agree in indicating that the total spin fraction carried by down-quarks is much smaller and near-zero compared to the up-quark and that the quarks account for about half of the proton spin.

* * *

We thank the SFB/TRR-55 for making available to us their gauge configurations for $\beta = 5.29$ and $\kappa = 0.1364$ ($m_\pi = 160\,\mathrm{MeV}$) via the ILDG. We have used HPC resources on the Jugene system at the research center in Jülich through PRACE and the Cy-Tera facility of the Cyprus Institute under the project Cy-Tera (NEA ΥΠΟΔΟΜΗ/ΣΤΡΑΤΗ/0308/31), first access call (project lspro113s1). This work is supported in part by the Cyprus Research Promotion Foundation under contracts TECHNOLOGY/ΘΕΠΙΣ/0311 (BE)/16, ΠΡΟΣΕΛΚΥΣΗ/ΝΕΟΣ/0609/16, and the Research Executive Agency of the European Union under Grant Agreement number PITN-GA-2009-238353 (ITN STRONGnet). K. J. was supported in part by the Cyprus Research Promotion Foundation under contract ΠΡΟΣΕΛΚΥΣΗ/ΕΜΠΕΙΡΟΣ/0311/16. KJ and VD acknowledge financial support by the DFG-funded corroborative research center SFB/TR9.

REFERENCES

[1] Alexandrou C., *PoS*, **LATTICE2010** (2010) 001 arXiv:1011.3660.
[2] Alexandrou C., *Prog. Part. Nucl. Phys.*, **67** (2012) 101 arXiv:1111.5960.
[3] Alexandrou C., Papanicolas C. and Vanderhaeghen M. arXiv:1201.4511.
[4] Alexandrou C. *et al.*, *PoS*, **LATTICE2012** (2012) 184 arXiv:1211.0126.
[5] Alexandrou C., Hadjiyiannakou K., Koutsou G., O'Cais A. and Strelchenko A., *Comput. Phys. Commun.*, **183** (2012) 1215 arXiv:1108.2473.
[6] Alexandrou C., Korzec T., Koutsou G. and Leontiou T. arXiv:1302.4410.
[7] Alexandrou C. *et al.* arXiv:1303.5979.
[8] Yamazaki T. *et al.*, *Phys. Rev. D*, **79** (2009) 114505 arXiv:0904.2039.
[9] Bratt J. D. *et al.*, *Phys. Rev. D*, **82** (2010) 094502 arXiv:1001.3620.
[10] Horsley R. *et al.* arXiv:1302.2233.
[11] Green J. *et al.*, *PoS*, **LATTICE2012** (2012) 170 arXiv:1211.0253.
[12] Dinter S. *et al.*, *Phys. Lett. B*, **704** (2011) 89 arXiv:1108.1076.
[13] Capitani S. *et al.*, *Phys. Rev. D*, **86** (2012) 074502 arXiv:1205.0180.
[14] Green J. *et al.* arXiv:1209.1687.
[15] Aoki Y. *et al.*, *Phys. Rev. D*, **82** (2010) 014501 arXiv:1003.3387.
[16] Pleiter D. *et al.*, *PoS*, **LATTICE2010** (2010) 153 arXiv:1101.2326.
[17] Bali G. S. *et al.*, *Phys. Rev. D*, **86** (2012) 054504 arXiv:1207.1110.